Science Bulletin 64 (2019) 756–763

Contents lists available at ScienceDirect

Science Bulletin

journal homepage: www.elsevier.com/locate/scib

Article

40-Year (1978–2017) human settlement changes in China reflected by impervious surfaces from satellite remote sensing

Peng Gong [a,b,c,*], Xuecao Li [d], Wei Zhang [a]

[a] Ministry of Education Key Laboratory of Earth System Modeling, Department of Earth System Science, Tsinghua University, Beijing 100084, China
[b] Tsinghua Urban Institute, Tsinghua University, Beijing 100084, China
[c] Center for Healthy Cities, Institute for China Sustainable Urbanization, Tsinghua University, Beijing 100084, China
[d] Department of Geological and Atmospheric Sciences, Iowa State University, Ames, IA 50011, USA

ARTICLE INFO

Article history:
Received 31 December 2018
Received in revised form 3 March 2019
Accepted 4 March 2019
Available online 18 April 2019

Keywords:
Urbanization
Rural development
Landsat data
Land cover change
Japan

ABSTRACT

Impervious surfaces are the most significant feature of human settlements. Timely, accurate, and frequent information on impervious surfaces is critical in both social-economic and natural environment applications. Over the past 40 years, impervious surface areas in China have grown rapidly. However, annual maps of impervious areas in China with high spatial details do not exist during this period. In this paper, we made use of reliable impervious surface mapping algorithms that we published before and the Google Earth Engine (GEE) platform to address this data gap. With available data in GEE, we were able to map impervious surfaces over the entire country circa 1978, and during 1985–2017 at an annual frequency. The 1978 data were at 60-m resolution, while the 1985–2017 data were in 30-m resolution. For the 30-m resolution data, we evaluated the accuracies for 1985, 1990, 1995, 2000, 2005, 2010, and 2015. Overall accuracies reached more than 90%. Our results indicate that the growth of impervious surface in China was not only fast but also considerably exceeding the per capita impervious surface area in developed countries like Japan. The 40-year continuous and consistent impervious surface distribution data in China would generate widespread interests in the research and policy-making community. The impervious surface data can be freely downloaded from http://data.ess.tsinghua.edu.cn.

1. Introduction

Impervious surfaces, as the major component of human settlements, are mainly artificial structures that are composed of any material that impedes or prevents natural infiltration of water into the soil. They include roofs, paved surfaces, hardened grounds mainly found in human settlements, and major road surfaces [1,2]. Mapping impervious surfaces with remotely sensed data onboard satellite has a long history [3–6]. Since Landsat data became freely accessible in 2008, a considerable amount of research has been made to map impervious surfaces (or urban land cover) using time series data [7–14] over all the world. Although a number of 300–1,000 m resolution urban extent maps were developed close to an annual basis [15,16], there exists a large uncertainty among those different urban layers due to source of data used, definition inconsistency, and mapping methods [7,17].

During 1978–2017, China has undergone economic reform and rapid urbanization. Significant land cover change has occurred in China [18]. For a number of applications such as regional scale urban development and management, study of air and water pollution, and climate change and biodiversity research, high-accuracy data on settlement change at the annual level with relatively high spatial resolution is badly needed for the entire country [19]. It is possible to collect enough Landsat data, acquired from the 1970s and onward, that enable us to map impervious surfaces as a surrogate of human settlements in China since the 1978 economic reform. However, thus far, settlement extent data in map forms only exist in every five years at best [20,21].

The purpose of this research was to develop an annual impervious surface map whenever the Landsat data were available between 1978 and 2017. In the remaining of this paper, unless stated otherwise, we shall make no distinction between human settlements and impervious surfaces as in our method we only extracted the later. In the following, we introduce the framework of method, report the result, and compare our results with existing urban layers developed by others.

* Corresponding author.
E-mail address: penggong@tsinghua.edu.cn (P. Gong).

https://doi.org/10.1016/j.scib.2019.04.024
2095-9273/

2. Method

We developed an automatic impervious surface mapping framework on Google Earth Engine (GEE), using our previously developed algorithms [12,22] (Fig. 1). They were successfully tested in mapping the annual growth of Beijing City and several other regions in China over 30 years. First, we divided China into 298 image grids, each with approximately 200 km × 200 km in size. Inside each grid, we collected training sample units in core-urban and rural areas based on Landsat observation in earlier years (1980s). Second, we collected all Landsat datasets in GEE and processed them through removing clouds (and their shadows). After that, we applied the developed "Exclusion/Inclusion" algorithm to generate initial maps of impervious surface in urban and surrounding rural areas [22]. Finally, we derived annual time series data of human settlements reflected by impervious surfaces after implementing the temporal consistency check algorithm [12]. All these algorithms were compiled in the GEE to ensure mapping efficiency at large scales.

Landsat imagery is our main source in this mapping project, with an ancillary dataset of nighttime light (NTL) data. The data source for the 1970 s is mainly from Landsat 1–3, of which the sensor is Multispectral Scanner (MSS) with a resampled pixel size of 60 m. Due to the limitation of data acquisition and data quality, annual coverage of MSS data is not possible in the 1970s. Fortunately, the settlement development in China, particularly urban development, was slow during that period. Thus we used data acquired around 1978 with complete coverage of China to extract settlements. For the remaining years, 30-m resolution images acquired on board Landsat 4, 5, 7, and Landsat 8 can mostly cover the entire country on an annual basis. The NTL data were derived from the Day/Night Band (DNB) detectors of the Suomi-NPP Visible Infrared Imaging Radiometer Suite (VIIRS) [23]. To mitigate uncertainties in mapped impervious surfaces, we used the NTL derived lit areas (annual mean of 2017) as a mask, for grids located in arid or semi-arid areas (i.e., west of Tengchong-Aihui line). We developed annual settlement layers from 1985 to 2017. In total, we have 34 settlement layers covering the entire 40-year time span.

We implemented different algorithms for the processing of the 60-m resolution MSS and 30-m resolution Landsat Thematic Mapper (TM), Enhanced Thematic Mapper Plus (ETM+), and Operational Land Imager (OLI) data. For MSS, we used the digital number (DN) values, which were calibrated through geometric and terrain correction. Clouds (and their shadows) were excluded using a threshold based approach proposed in [24]. For TM, ETM +, and OLI, we used the surface reflectance data, which had been processed with geometric, terrain, and radiometric corrections and identified cloudy regions [25]. We systematically corrected the OLI surface reflectance data to make it consistent with other sensors (i.e., TM and EMT+) [26]. For each year, we used all images acquired from the green season (June-August) for image composition, through filling each pixel with the data that have the highest Normalized Difference Vegetation Index (NDVI) among those images. Comparing to widely used mean or median strategies, our composition can substantially reduce the effect of the scanline drop-off issue in Landsat 7 images (e.g., ETM+) since 2003.

We classified the initial impervious surface areas using training sample units collected in core-urban and rural areas in earlier years (1980s), and derived annual impervious surface dynamics (1985–2017) with the consideration of temporal consistency of urban development (Fig. 2). The adopted sample collection strategy (Fig. 2a) ensures (1) a sample unit would remain as an impervious surface in subsequent years because for most places development is irreversible; (2) each sample unit can be spatially extended (i.e., 3 × 3 pixels) to more sample units for training [27]. For each year, we mapped initial impervious surface extent using NDVI, modified normalized difference water index (MNDWI), and shortwave infrared (SWIR) data extracted from Landsat images using the "Exclusion-Inclusion" approach [22] (Fig. 2b). Thresholds used for impervious surface mapping are determined for each mapping year. Masks derived from the time-series data and NTL data were used as spatial constraints to derive impervious surfaces (Fig. 2c). This helps reduce potential confusion between impervious cover and bare land, particularly in arid and semi-arid areas. Given that mean values of such indices as NDVI, MNDWI, and SWIR are different in urban and rural areas, thresholds were separately

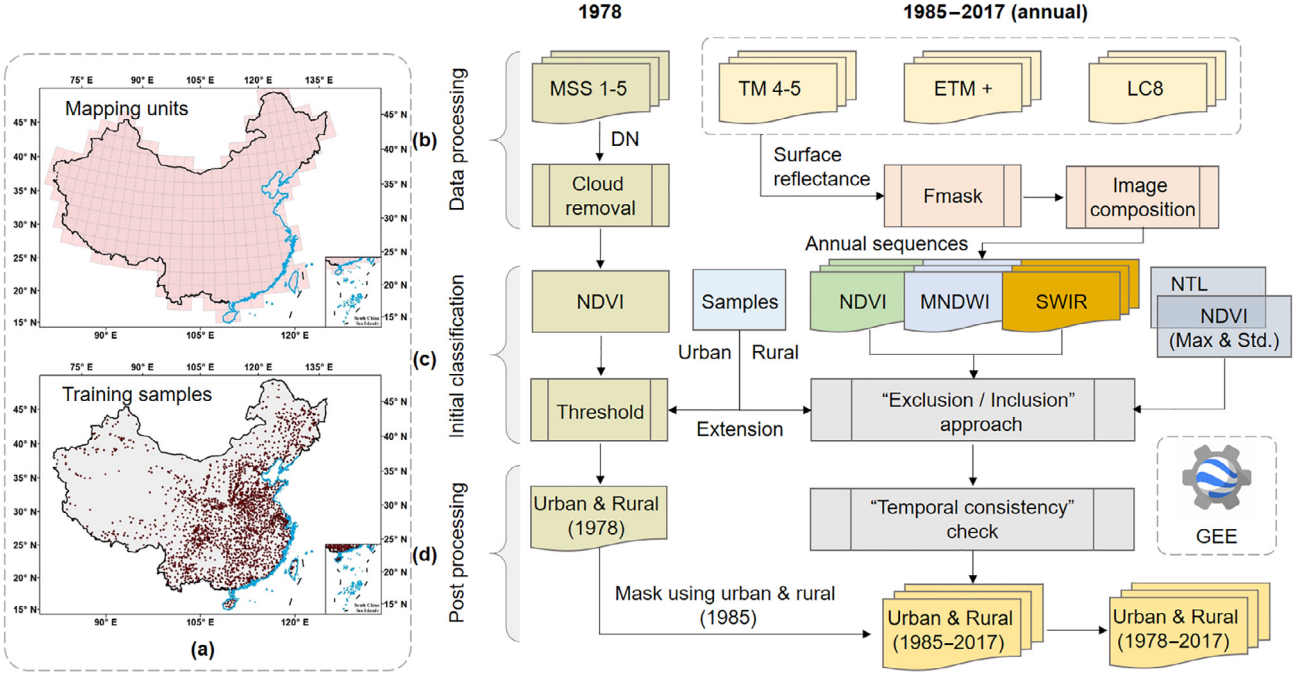

Fig. 1. Flowchart of mapping procedures in this study. (a) Mapping unit and training samples; (b) data processing of Landsat images; (c) initial classification of annual urban/rural areas; (d) temporal consistency check of derived time series data.

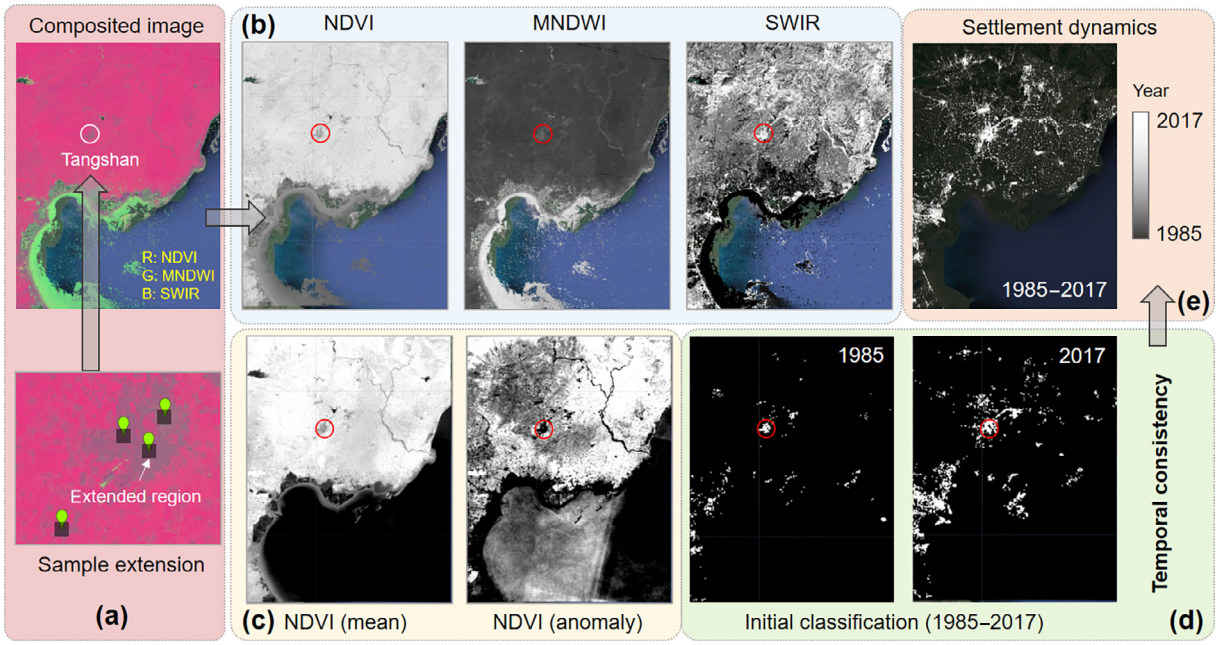

Fig. 2. Illustration of generating annual urban impervious surface using Landsat time series data. (a) Image composition and sampling (1985); (b), (c) main and ancillary features used for initial classification; (d) temporal consistency; (e) derived annual settlement dynamics reflected by the impervious surfaces. The city within circles is Tangshan. NTL data is not included here because they were used for arid and semi-arid regions. Features in (c) were derived using all time-series data within a year.

determined to extract time-series urban and rural settlements using collected urban and rural sample units, respectively. We then applied "temporal consistency check" (Fig. 2d), which consists of temporal filtering and logistic reasoning, on the initial classification results [12]. That is, misclassified impervious surface of individual years caused by poor-quality Landsat images were modified using results from temporally neighboring years. Also, the derived time series data follow the development logic – only from undeveloped land to impervious surface. Finally, we derived annual settlement dynamics from the impervious data in urban and rural areas from 1985 to 2017 (Fig. 2e). For 1978, we mapped the settlement extent from the composite NDVI layer (from MSS) using the same approach, and the resultant settlement extent in 1978 was further constrained using the settlement extent of 1985.

3. Results and validations

The derived impervious surfaces well reflect the urbanization process over the period of four decades (Fig. 3). In 1978, settlements were mainly located in the urban center in an aggregated form. Thereafter, they were spatially expanded from urban core at an unprecedented rate, particularly after 2000. In addition, these newly urbanized regions are more spatially disaggregated when compared to earlier settlements. In particular, Shenzhen had hardly any settlement in 1978, and its dynamics matches well with the "opening and reform" policy.

We developed a validation sample set from interpretation, using time series data and high resolution images. Based on our annual impervious surface sequence, we extract strata of (1) non-urban; (2) urbanized in 1985; (3) urbanized during 1985–1990; (4) urbanized during 1990–1995; (5) urbanized during 1995–2000; (6) urbanized during 2000–2005; (7) urbanized during 2005–2010; and (8) urbanized during 2010–2015 (Fig. S1a online). Each contains 100 sample units randomly located in the corresponding stratum. Identification on whether or not a sample unit is an impervious surface is based on manual interpretation of a long-term NDVI time series, local views of Landsat images, and high resolution Google Earth Images (Fig. S1b online). For accuracy assessment, we used the non-urban stratum and urban stratum for different years (Table 1). The average overall accuracy (OA) is 93.42% over these seven periods. In general, accuracies in earlier periods are higher. Most errors are caused by confusion between barren areas and urban lands according to the interpretion result.

We also validated the results with locations in geoNames (http://download.geonames.org) due to its nearly full coverage of human settlements with different sizes in the world. Each sample location reflects a point falling in a town or city. The validation is done to the 2017 settlement map. Out of the 2,354 sample locations (Fig. 4), 2,039 fell inside our impervious surface areas (87%). It can be seen that the coastal areas were accurately mapped. Only Inner Mongolia, Qinghai, Tibet, Xijiang, and Yunnan provinces have lower than 70% accuracies. The low accuracies in western China fall in arid (or semi-arid), cold, and highly mountainous regions in China. It implies that nightlight data are not strong enough to help preserve settlements in those areas.

We also compared 1990, 2000, and 2010 mapped settlement areas with the same year manual interpretation urban extent maps for all 650 cities in China [7]. With the urban extent masks we randomly selected 14,268, 15,220 and 17,760 sample locations from the 1990, 2000, and 2010 layers, respectively. The overall agreement of these three years are 78.28%, 79.13% and 80.08%, respectively. This shows our mapping results are fairly consistent. As the urban extent data were manually delineated to encompass a connected urban area including vegetation, water surfaces and other non-impervious surfaces, the approximately 80% agreement does not mean that it was the accuracy of our map products because there is a chance that our selected sample locations fall into vegetation or water within the urban extent maps manually delineated.

There is an overall trend of settlement expansion in every province in China (Fig. 5). By 2017, the top urban expansion provinces are Shandong, Jiangsu, Hebei, Guangdong, and Henan. At the total rural and urban expansion level, the order of the top 3 remains the same but the 4th and 5th became Henan and Anhui. These indicate the high level of land development in eastern China. Guangdong may be limited by its high proportion of relief terrain and other

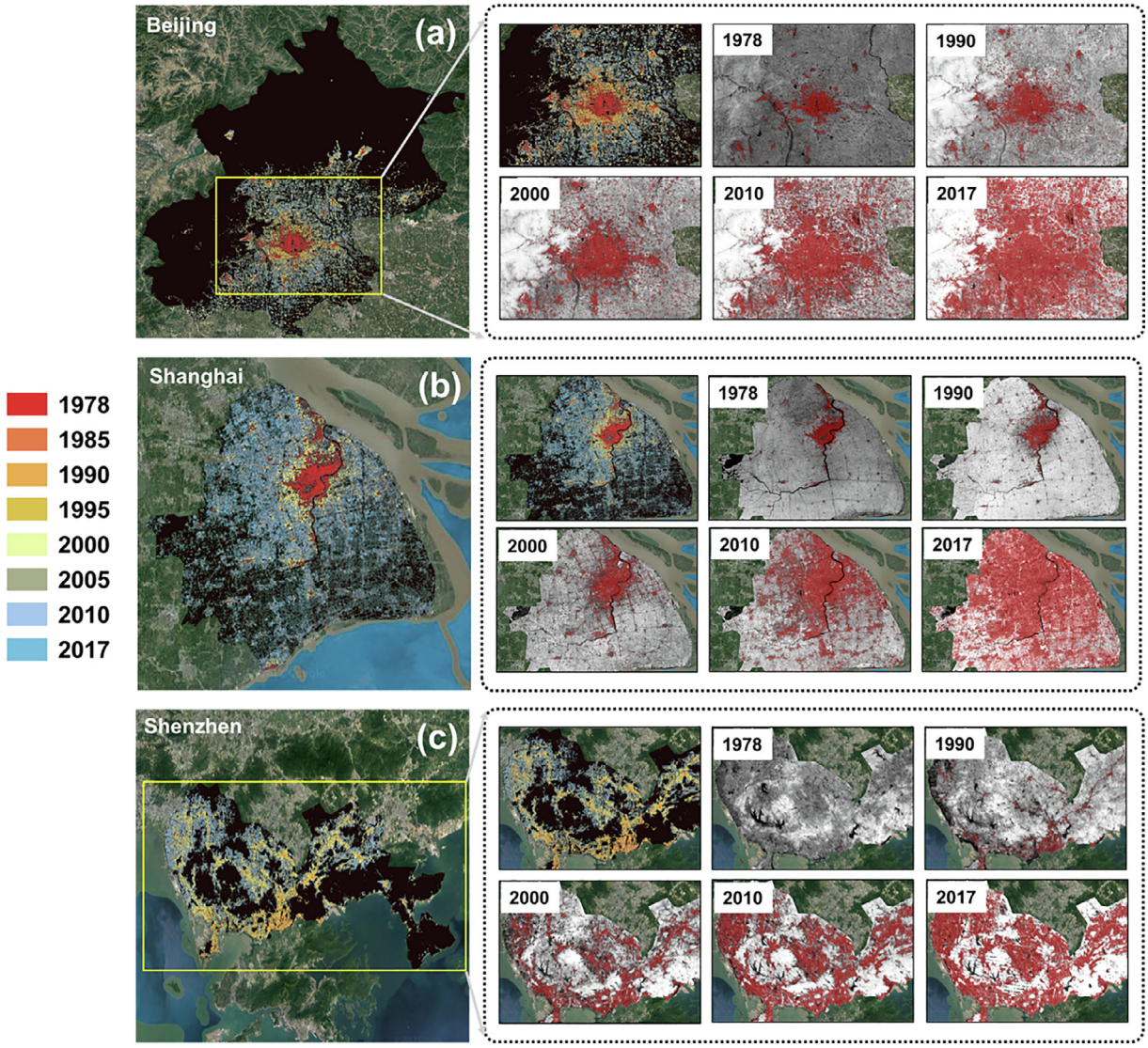

Fig. 3. Illustration of extracted settlements for Beijing (a), Shanghai (b), and Shenzhen (c). Grey images in dotted frames are NDVI of different years overlaid settlement extraction in red.

Table 1
Accuracy table for each mapping time intervals.[a]

Year		Non-urban	Urban	PA (%)	Year	Non-urban	Urban	PA (%)
1985	Non-urban	99	1	99	1990	99	1	99
	Urban	10	90	90		13	87	87
	UA (%)	91	99			88	99	
	OA (%)	94.5	Kappa	0.89		93	Kappa	0.86
1995	Non-urban	99	1	99	2000	99	1	99
	Urban	8	92	92		9	91	91
	UA (%)	93	99			92	99	
	OA (%)	95.5	Kappa	0.91		95	Kappa	0.9
2005	Non-urban	99	1	99	2010	99	1	99
	Urban	15	85	85		13	87	87
	UA (%)	87	99			88	99	
	OA (%)	92	Kappa	0.84		93	Kappa	0.86
2015	Non-urban	99	1	99				
	Urban	17	83	83				
	UA (%)	85	99					
	OA (%)	91	Kappa	0.82				

[a] UA: users' accuracy; PA: producer's accuracy; OA: overall accuracy.

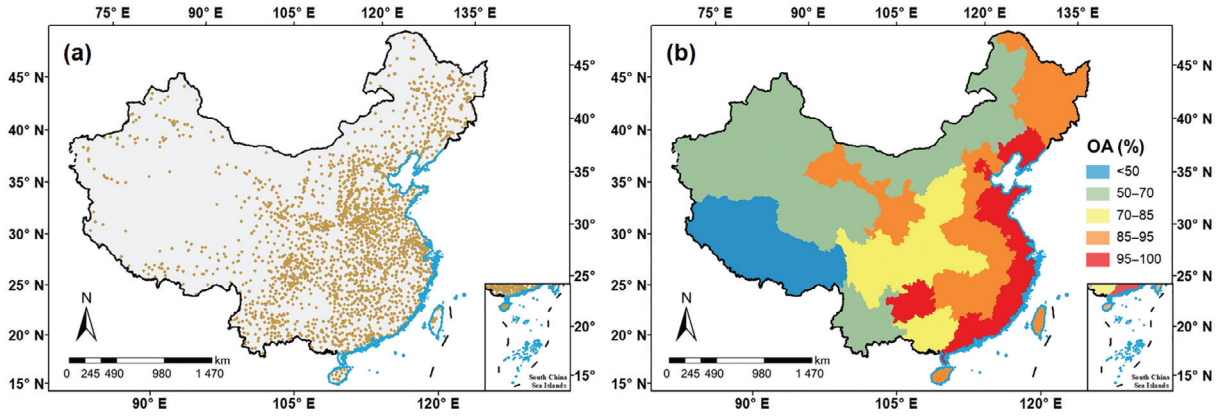

Fig. 4. Distribution of geoNames samples (a) for accuracy assessment (b).

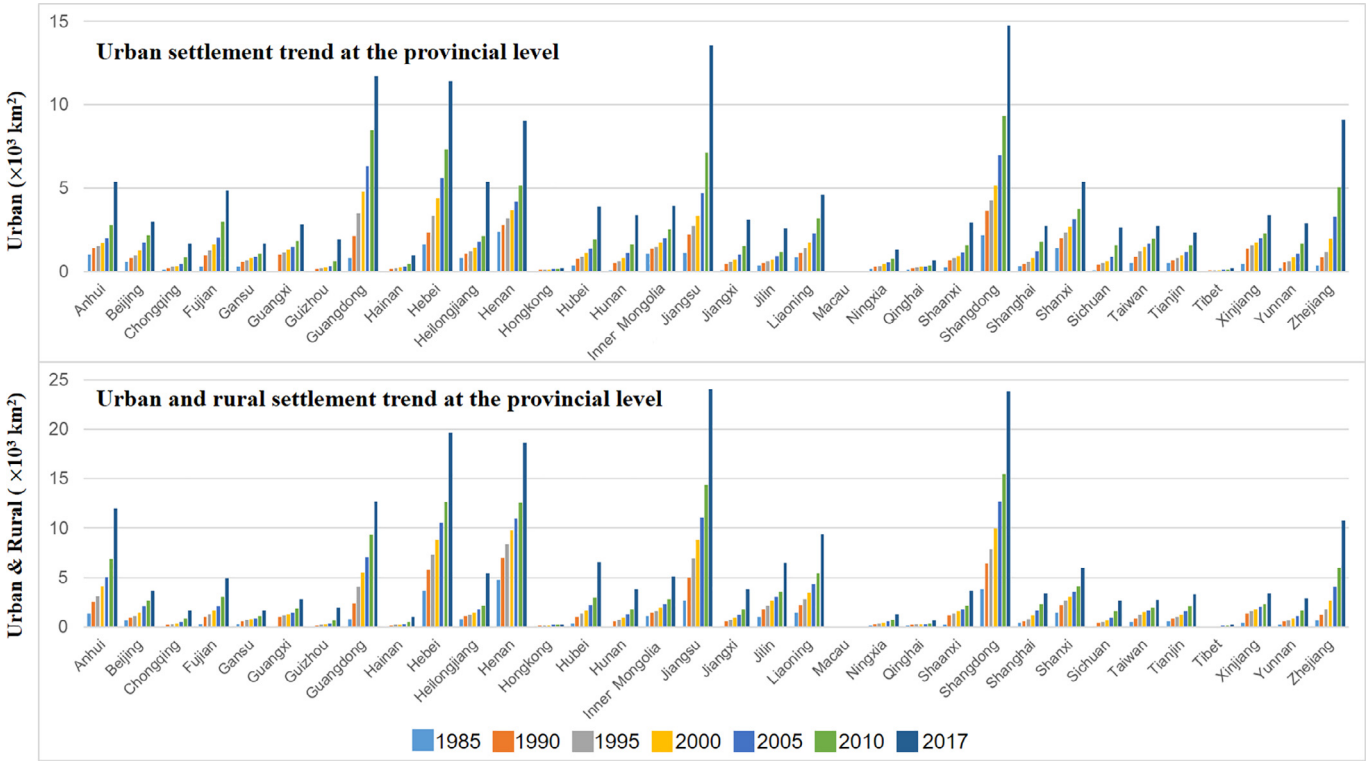

Fig. 5. Settlement change trends from 1985 to 2017 by provinces.

socio-economic constraints. In total, by 2017, the urban settlement areas reflected by impervious surfaces in China were 146,102 km^2, while the urban and rural as a whole was 209,950 km^2, approximately 13.6 times of the 15,364 km^2 mapped in 1978.

Taking as the base the 1980s land cover and land use map of China developed by the Institute of Geographic Sciences and Natural Resources Research of Chinese Academy of Sciences [20], we overlaid the impervious surface growth maps on top of it, the sources of different land cover and land use types that were converted into impervious surfaces can be estimated (Fig. S2a online). The expansion of impervious surface area occupied about 147,551 km^2 of natural lands. Among this, 80% were originally agricultural land, 8.1% converted from forested land, 6.6% came from grassland. At the provincial level, the contribution of cropland to impervious surface in 2017 has been shown in Fig. S2b (online). Jiangsu, Shandong, Hebei, Henan, and Anhui are among the top five. More than 15,000 km^2 croplands have been lost in Jiangsu.

Our results can be compared with several existing settlement data layers, the 300-m resolution Global Human Settlement (GHS) [16] and the 30-m resolution manually interpreted national land cover dynamics layers (NLCD) in every five years [20] (Fig. 6). While more systematic comparison can be done by users, our preliminary comparison indicates that our results are the most balanced in rural and urban impervious surface mapping. For example, the manually interpreted NLCD is not pixel-based and the level of generalization is particularly variable in rural areas. The GHS data omit rural settlements in some cities in central China (e.g., Xi'an).

Japan is a country with similar climate to eastern China and it had experienced a long-term urbanization. We applied the same method to completely map impervious surfaces in Japan over 1985–2017. Japan's land development rate as measured by impervious surface growth is considerably different from China. Compared with 1990, China's grown impervious surface tripled by

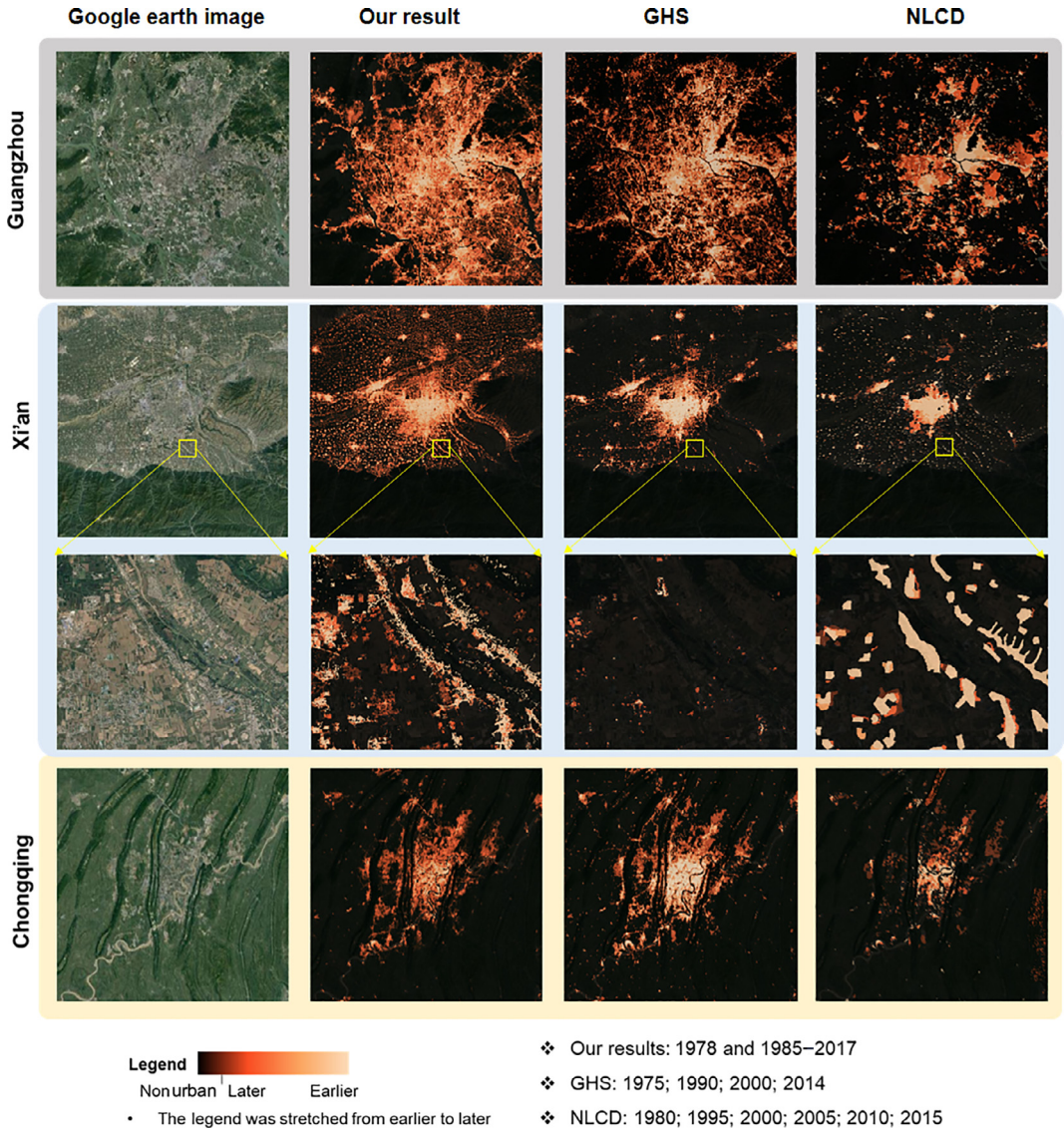

Fig. 6. Comparison of Guangzhou, Xi'an, and Chongqing in different products. Our results are human settlements in both urban and rural areas.

2017 while it was only 96% in Japan (Fig. S3 online). By 2017, the total impervious surface area in China has been 209,950 km^2 while in Japan this value was 14,290 km^2, 6.8% of China's total. The 2017 per capita impervious surface area of Chinese people (151.7 m^2) was 35% more than that of Japanese people (112.7 m^2). China's over-expansion in land development is worthy of deeper analysis.

4. Discussion

Our method cannot detect vegetation-covered impervious surface areas due to the top-down view of satellite data used in this study. On the other hand, there could also be bias due to mixed pixel effect in urban areas. Since the 30-m resolution pixel in Landsat images is still considerably greater than many man-made structures, our method has to deal with the problem that a large proportion of pixels in human settlement areas is spectral mixture of impervious surface, green space, water and soil cover types. If the spectral contribution of impervious surfaces are heavily weighted in a pixel, the chance for a pixel to be identified as impervious surface would be high although this over-weighting effect maybe cancelled out by pixels dominated by green space or other non-impervious surfaces. The effect of spectral mixture problem on the extraction of impervious surface from mixed pixels in Landsat data cannot be properly evaluated until a careful comparison with impervious surfaces extracted with sub-meter resolution data over various human settlement areas is done. Instead, we did some comparison with several existing data products in the following.

Overall, our human settlement dynamics reflected by the impervious surface agree with other existing urban extent products (Table 2), although their definitions, methods, and satellite data sources may be different. The NLCD includes artificial surfaces both in urban and rural areas, and it is comparable with our results. Our estimation of total settlements in 2015 and 2010 are 186,227 and 127,512 km^2, respectively, which are lower than NLCD (227,792 and 198,653 km^2). It should be noted that NLCD does not distinguish impervious surfaces from its human settlement land use classes. For human settlements in urban areas, our estimations in 1995 and 2000 are in the middle of results derived from GHS and a night-time light based urban dynamics product NTLUD [28]. However, our result is the highest in 2015 with an area of 131,719 km^2. From the temporal perspective, the rate of urban settlement increment in 2015 relatively to 1995 is 2.26 in our result, while it is 0.75 and 4.25 in GHS and NTLUD derived results,

Table 2
Comparison of some human settlement products over China.

Year	This study (urban and rural)	NLCD	GHS	This study (urban)	NTLUD
1995	65,117	168,331	60,950	40,405	24,917
2000	80,989	173,357	76,929	49,863	35,294
2005	100,106	189,105		64,003	55,879
2010	127,512	198,653		86,673	91,075
2015	186,227	227,792	106,947	131,719	130,916

respectively. The GHS results are likely to underestimate the urban growth over past decades, because the built-up areas increased more than 2 times during the period of 1990–2010, based on human interpreted results [7]. In addition, it is reasonable for our increment to be lower than NTLUD results since less light was emitted from cities in earlier years.

Uncertainty exists both in time and space in our product. Although we used NTL data as a mask to delineate human settlement boundaries in arid and semi-arid regions, the confusion between impervious surfaces and barren (e.g., rock or dry soil) is a primary difficulty due to similar spectral signatures. This issue has been widely reported in other studies [9,12,21]. Change information derived from time series analysis can be regarded as a complement to reduce the spectral confusion in future attempts [29]. Also, there are limited good-quality Landsat images in earlier years (e.g., circa 1980s), which is an additional source of uncertainty in our product. For example, the Landsat MSS data had fewer bands and were not converted into reflectance data, which is different from those in Landsat TM, ETM+, and OLI data. This issue cannot be fully resolved due to the limitation of historical data, even although we have done temporal consistency check.

5. Conclusions and perspectives

China has undergone rapid land development during the past 40 years. We developed the first annual human settlement map from 1985 to 2017 with a circa 1978 map produced at the beginning of the economic reform in China. Checking against our own validation sample the overall accuracy exceeded 90% but with an imbalance of the eastern coastal areas higher than the interior regions. Between 1978 and 2017, over 118,205 km^2 of croplands were converted into impervious surfaces. Considering that impervious surfaces were only one part of the urbanization, it is clear that this is a lower end of estimate on China's agricultural land conversion to urban areas. The total human settlement area exceeded 209,950 km^2 which is bigger than the size of United Kingdom. Compared with Japan, China's per capita settlement is over 35% more in 2017.

The growth trend of settlements will continue in China at a rapid pace before 2030 [30–32]. There is continuing needs for frequent monitoring of human settlement growth. However, the method presented here is less accurate in less developed arid and cold regions in China. Occupying a small portion of the land area on Earth, human settlement mapping is proven difficult in automatic general-purpose land cover mapping [33]. As can be seen from our comparison with manual interpretation results, small human settlements are poorly delineated in manual interpretation results. It is important to incorporate new sources of data and explore new mapping algorithms [19,34–37]. Only with consistently accurate, high resolution and frequent monitoring of human settlement areas can it be possible to meet the data needs in urban planning and management, beautiful and specialized village and township development, and many other applications including climate change, energy conservation, and environment protection in China [38–40]. The framework developed here can be extended to mapping the entire world in the GEE platform [41].

Conflict of interest

The authors declare that they have no conflict of interest.

Acknowledgments

This work was partially supported by the National Research Program of the Ministry of Science and Technology of China (2016YFA0600104), and donations from Delos Living LLC and the Cyrus Tang Foundation to Tsinghua University. Maps in this article were reviewed by Ministry of Natural Resources of the People's Republic of China (GS(2019)1344)).

Author contributions

Peng Gong conceived and supervised the research topic; Xuecao Li and Wei Zhang performed the experiments and analyzed the data; Peng Gong wrote the paper.

Appendix A. Supplementary data

Supplementary data to this article can be found online at https://doi.org/10.1016/j.scib.2019.04.024.

References

[1] Angel S, Parent J, Civco DL, et al. The dimensions of global urban expansion: estimates and projections for all countries, 2000–2050. Progr Plann 2011;75:53–107.
[2] Bounoua L, Nigro J, Zhang P, et al. Mapping urbanization in the United States from 2001 to 2011. Appl Geogr 2018;90:123–33.
[3] Jensen JR, Toll DL. Detecting residential land-use development at the urban fringe. Photogramm Eng Remote Sens 1982;48:629–43.
[4] Howarth PJ, Boasson E. Landsat digital enhancements for change detection in urban environments. Remote Sens Environ 1983;13:149–60.
[5] Lo CP. Chinese settlement pattern-analysis using Shuttle Imaging Radar-A data. Int J Remote Sens 1984;5:959–67.
[6] Forster BC. An examination of some problems and solutions in monitoring urban areas from satellite platforms. Int J Remote Sens 1985;6:139–51.
[7] Wang L, Li CC, Ying Q, et al. China's urban expansion from 1990 to 2010 determined with satellite remote sensing. Chin Sci Bull 2012;57:2802–12.
[8] Wang J, Li CC, Hu LY, et al. Seasonal land cover dynamics in Beijing derived from Landsat 8 data using a spatio-temporal contextual approach. Remote Sens 2015;7:865–81.
[9] Song XP, Sexton JO, Huang CQ, et al. Characterizing the magnitude, timing and duration of urban growth from time series of Landsat-based estimates of impervious cover. Remote Sens Environ 2016;175:1–13.
[10] Huang HB, Chen YL, Clinton N, et al. Mapping major land cover dynamics in Beijing using all Landsat images in Google Earth Engine. Remote Sens Environ 2017;202:166–76.
[11] Cao H, Liu J, Fu C, et al. Urban expansion and its impact on the land use pattern in Xishuangbanna since the reform and opening up of China. Remote Sens 2017;9:137.
[12] Li XC, Gong P, Liang L. A 30-year (1984–2013) record of annual urban dynamics of Beijing City derived from Landsat data. Remote Sens Environ 2015;166:78–90.
[13] Andrade-Nunez MJ, Aide TM. Built-up expansion between 2001 and 2011 in South America continues well beyond the cities. Environ Res Lett 2018;13.
[14] Mohammad Mehedy H, Jane S. Analyzing land cover change and urban growth trajectories of the mega-urban region of dhaka using remotely sensed data and an ensemble classifier. Sustainability 2018;10:10.
[15] Schneider A, Friedl MA, Potere D. A new map of global urban extent from MODIS satellite data. Environ Res Lett 2009;4.

[16] Melchiorri M, Florczyk AJ, Freire S, et al. Unveiling 25 years of planetary urbanization with remote sensing: perspectives from the global human settlement Layer. Remote Sens 2018;10:768.
[17] Seto KC, Fragkias M, Guneralp B, et al. A meta-analysis of global urban land expansion. PLoS One 2011;6.
[18] Xu N, Gong P. Significant coastline changes in China during 1991–2015 tracked by Landsat data. Sci Bull 2018;63:883–6.
[19] Zhang ZX, Liu F, Zhao XL, et al. Urban expansion in China based on remote sensing technology: a review. Chin Geogr Sci 2018;28:727–43.
[20] Liu JY, Kuang WH, Zhang ZX, et al. Spatiotemporal characteristics, patterns, and causes of land-use changes in China since the late 1980s. J Geogr Sci 2014;24:195–210.
[21] Liu XP, Hu GH, Chen YM, et al. High-resolution multi-temporal mapping of global urban land using Landsat images based on the Google Earth Engine Platform. Remote Sens Environ 2018;209:227–39.
[22] Li XC, Gong P. An, "exclusion-inclusion" framework for extracting human settlements in rapidly developing regions of China from Landsat images. Remote Sens Environ 2016;186:286–96.
[23] Elvidge CD, Baugh K, Zhizhin M, et al. VIIRS night-time lights. Int J Remote Sens 2017;38:5860–79.
[24] Braaten JD, Cohen WB, Yang Z. Automated cloud and cloud shadow identification in Landsat MSS imagery for temperate ecosystems. Remote Sens Environ 2015;169:128–38.
[25] Zhu Z, Woodcock CE. Object-based cloud and cloud shadow detection in Landsat imagery. Remote Sens Environ 2012;118:83–94.
[26] Roy DP, Kovalskyy V, Zhang HK, et al. Characterization of Landsat-7 to Landsat-8 reflective wavelength and normalized difference vegetation index continuity. Remote Sens Environ 2016;185:57–70.
[27] Li C, Gong P, Wang J, et al. The first all-season sample set for mapping global land cover with Landsat-8 data. Sci Bull 2017;62:508–15.
[28] Zhou YY, Li XC, Asrar GR, et al. A global record of annual urban dynamics (1992–2013) from nighttime lights. Remote Sens Environ 2018;219:206–20.
[29] Li XC, Zhou YY, Zhu ZY, et al. Mapping annual urban dynamics (1985–2015) using time series of Landsat data. Remote Sens Environ 2018;216:674–83.
[30] Shi KF, Chen Y, Yu BL, et al. Urban expansion and agricultural land loss in china: a multiscale perspective. Sustainability 2016;8:790.
[31] Wang J, Zhang WW, Zhang ZX. Quantifying the spatio-temporal dynamics of rural settlements and the associated impacts on land use in an undeveloped area of China. Sustainability 2018;10:1490.
[32] Yang J, Wu TH, Gong P. Implementation of China's new urbanization strategy requires new thinking. Sci Bull 2017;62:81–2.
[33] Gong P, Wang J, Yu L, et al. Finer resolution observation and monitoring of global land cover: first mapping results with Landsat TM and ETM+ data. Int J Remote Sens 2013;34:2607–54.
[34] Hu TY, Yang J, Li XC, et al. Mapping urban land use by using Landsat images and open social data. Remote Sens 2016;8:151.
[35] Lyu HB, Lu H, et al. Long-term annual mapping of four cities on different continents by applying a deep information learning method to Landsat data. Remote Sens 2018;10:471.
[36] Huang X, Hu T, Li JY, et al. Mapping urban areas in china using multisource data with a novel ensemble SVM method. IEEE Trans Geosci Remote 2018;56:4258–73.
[37] Li XC, Gong P. Urban growth models: progress and perspective. Sci Bull 2016;61:1637–50.
[38] Yang J, Gong P, Fu R, et al. The role of satellite remote sensing in climate change studies. Nat Clim Change 2013;3:875–83.
[39] Zhang GJ, Cai M, Hu AX. Energy consumption and the unexplained winter warming over northern Asia and North America. Nat Clim Change 2013;3:466–70.
[40] Yu CQ, Huang X, Chen H, et al. Managing nitrogen to restore water in China. Nature 2019;567:516–20.
[41] Guo H, Wang L, Liang D. Big Earth Data from space: a new engine for Earth science. Sci Bull 2016;61:505–13.

Peng Gong is currently a professor and chair of the Department of Earth System Science and the dean of School of Sciences at Tsinghua University. His major research interests include mapping and monitoring of global environmental change using satellite and ground based sensors, and modelling of environmentally related infectious diseases.